ADVANCED SENSOR RESEARCH Open Access
www.advsensores.com

Towards Neural-Network-Based Optical Temperature Sensing of Semiconductor Membrane External Cavity Laser

*Jakob Mannstadt and Arash Rahimi-Iman**

A machine-learning (ML) non-contact method to determine the temperature of a laser gain medium via its laser emission with a trained few-layer neural-network (NN) model is presented. The training of the feed-forward NN enables the prediction of the device's properties solely from spectral data, here recorded by visible-/nearinfrared-light (VIS/NIR) compact micro-spectrometers for both a diode pump laser and optically-pumped gain membrane of a semiconductor disk laser. Fiber spectrometers are used for the acquisition of large quantities of labeled intensity data, which can afterwards be used for the prediction process. Such pretrained deep NNs enable a fast, reliable and easy way to infer the temperature of a laser system such as our Membrane External Cavity Laser, at a later monitoring stage without the need of additional optical diagnostics or read-out temperature sensors. With the miniature mobile spectrometer and the remote detection ability, the temperature inference capability can be adapted for various laser diodes using transfer learning methods with pretrained models. Here, mean-square-error (*mse*) values for the temperature inference corresponding to sub-percent accuracy of our sensor scheme are reached, while computational cost can be saved by reducing the network depth at the here displayed cost of accuracy, as appropriate for different application scenarios.

1. Introduction

The development and the design of various optical sensors has facilitated the monitoring of chemical compositions,[1] the human physiology,[2] temperature in technical installations[3] and detection of anomalies, e.g., caused by fire,[4] to name but a few.

Optical temperature sensors often rely on the reflection, propagation or interference of light that directly shines onto the object of which the temperature shall be determined. A number of different techniques are known in this domain, such as those using distributed Bragg gratings, Fabry–Perot microcavities or Raman and Rayleigh scattering.[5,6] Fiber Bragg Gratings are based on the wavelength shift of the peak reflectivity due to temperature-dependent refractive index changes. Consequently, the change of the wavelength can be employed as a temperature measure. In Fabry–Perot Interferometer the change of the relative distance of the mirrors due to the thermal expansion is employed. Thus, the peak transmission wavelength indicates the temperature in this type of sensor. Sensing methods that rely on direct backscattering of light from the target for instance are based on Raman scattering, where the ratio of anti-Stokes and Stokes scattered light powers is temperature dependent.[6]

In contrast, regarding light emitter devices, one can directly access thermal shifts for sensing properties. The quantum defect and other LASER device or LED inefficiencies will heat up the optical emitter system, which can cause a red shift on the emission wavelength, e.g., of the laser (gain spectrum). Such red shift can be employed to deduce the temperature of the emitter system. In semiconductor lasers, it arises mainly due to shift in the gain spectrum of the quantum well (QW) induced by a change in the band gap of the gain material. In addition, a rise in temperature thermally expands the typically employed microcavity of the laser system, generating another red shift of the emission wavelength. However, the change due to the gain spectrum of the QW dominates over the thermal expansion of the cavity.[7,8] The resulting overall output modification can be a suitable indicator of the device temperature.

To analyze the optical response, i.e., the light signal alterations according to the sensing principle, complex or expensive tools are typically employed, such as to probe wavelength shifts, pulse properties, signal levels, and so forth. Thus, they require some form of specialized detector or other additional devices to fulfil one or more tasks.

In contrast to aforementioned methods, techniques can be used which deduce temperature changes in an active medium by modifications of its irradiation properties.[9,10] Here, instead of having a mechanical or electronic sensor head in touch with the emitter medium, its emission properties are directly addressed and evaluated. This can be beneficial in situations, where

J. Mannstadt, A. Rahimi-Iman
I. Physikalisches Institut and Center for Materials Research
Justus-Liebig-Universität Gießen
35392 Gießen, Germany
E-mail: arash.rahimi-iman@exp1.physik.uni-giessen.de

The ORCID identification number(s) for the author(s) of this article can be found under https://doi.org/10.1002/adsr.70009

DOI: 10.1002/adsr.70009

sensor contact to the emitter is not conceivable. Accordingly, no additional extra optical information transfer link for the readout and no separate temperature sensors for temperature monitoring are needed.

At the example of a semiconductor gain medium under laser operation, we demonstrate the analysis of its temperature by detection and evaluation of its specific spectral signal changes. In this context, such a "thermal fingerprint" represented by the direct and clear dependence of a semiconductor disk laser's spectral signature on the device's temperature is used in this work for the training of multilayer feed-forward NN models towards a temperature sensor based on the laser's signal. Because the emitter system is usually thermally coupled to its environment, such as the substrate or carrier, which in most cases is considered as the heatsink's body, or the local part of a photonic chip etc., it can be considered as a sensing device. The direct analysis of collected laser light from the "optical sensor" device can be used for long-time temperature observation of far away lasers or remote objects that carry a laser, for which the spectral shift arises due to temperature differences with regard to the device's reference temperature. Our concept enables a non contact and long-distance examination of a gain-medium temperature and therewith a pathway to semiconductor-technology based miniaturized sensor elements, which for instance can be remotely probed by merely a simple miniaturized spectrometer coupled to a ML model.

Here, we investigated two lasers, which emit in the NIR spectral range at around 800 and 1070 nm, respectively, with a compact NN architecture after hyperparameter optimization. Particularly, the detection was pursued with two cost-effective miniature spectrometers, which span spectrally-different wavelength regions between 400 and 1700 nm. In this work, we demonstrate the temperature deduction performance for our most performant example configuration.

2. Experiment and Computational Methods

In order to acquire sufficiently enough data to train an NN, three spectrometers of similar type are employed for capturing labeled spectra at the same time - by that providing a connection between the three equally labeled captures. With the help of three similar yet different spectrometers owing to their different wavelength ranges, signal to noise ratios and their manufacturing-related deviations, it is possible to provide the network with slightly different spectra to prevent the network from overfitting and increase the robustness of our model. These spectrometers employed were deemed suitable to capture the laser signal due to their device characteristics. Therefore, the chosen spectrometer should have an appropriate resolving power of the emission line and a high signal to noise ratio. Moreover, concerning machine learning tasks, they should enable facile software integration and rapid data acquisition capacity for lab-task-tailored big data collection and processing. To fulfil these requirements, spectrometers of the type *PEBBLE* from *IBSEN Photonics*[11] are chosen.

Figure 1 sketches the experimental setup for the ML process principle for temperature regression by a trained NN. The emission spectra of the laser system are captured by the spectrometer and are labelled with their corresponding temperature according to the digital read-out of the respective heat sink temperature. Afterwards, the prepared spectra are delivered for use as the input to the NN. In the training process, the regressor-type NN model learns to map the input values to a temperature as part of a supervised learning setting for the prediction task. After the learning process, the network can predict the temperature merely based on a later provided input spectrum.

In this aforementioned setup there are two crucial issues for the task. Firstly, the proper spectra acquisition with the correct label, and secondly, the preparation of the data for the NN. **Figure 2** with its more detailed representation of the data acquisition configuration addresses the first point. Note that this sketch shows quite accurately where the fibers, laser, powermeter sensor head and so forth are placed during the measurement, using the optical setup's geometrical arrangement, and locates core items – other than the peripherical tools – properly and in proportion to the cm positions on the table. However, the actual placements were done arbitrarily and, accordingly, the arrangement could have been chosen differently as well.

Both visible-light spectrometers depicted (*PEBBLE* "VIS 1" and "VIS 2") cover a wavelength range between 400 and 1100 nm with a typical spectral resolution of 8 nm for the incorporated entrance slit width and type of transmission grating. The line-array detector in these spectrometers is a *Hamamatsu S14739*.[12] The near infrared spectrometer (*PEBBLE* "NIR") covers a spectral range between 900 and 1700 nm with a specified spectral resolution of approximately 12 nm owing to the given set of incorporated transmission grating and line-array detector for infrared signals. This type of NIR spectrometer has a *Hamamatsu G13913* detector.[13] Fiber 1 is connected to VIS *PEBBLE* 1 and points from behind the Membrane External Cavity Surface Emitting Laser (MECSEL) device[14] towards the overall open-cavity optically-pumped laser system and thus effectively collects stray light originating from both the pump laser and the MECSEL. Fiber 2 similarly does, though at a different ratio in peak intensities, and is connected to a fiber-type 50: 50 splitter, which guides the light to both the VIS *PEBBLE* 2 and the NIR *PEBBLE*. Due to the focus on MECSEL signal, and because the NIR *PEBBLE* does not detect pump-laser light, fiber 2 is located rather next to the laser system, but pointing also in the direction of the laser beam blocked by the power-meter sensor head to collect stray light predominantly from the outcoupled MECSEL beam after a long pass filter, which attenuates the pump laser light in the laser's external beam path. Nonetheless, the positions for both fiber tips (detecting facets) are chosen arbitrarily with the aim to record spectra with meaningful signal strength variations for the laser system, to artificially create and mimic power variations for the detected laser lines. In this work, we deliberately chose to develop a power-independent model, primarily with remote sensing applications in mind—where access to the detection point may be limited or restricted. In such scenarios, real-time knowledge of the actual pump power may not be available or reliable, making it challenging to incorporate it effectively for inference. In other use cases, e.g., where spectral intensity relationships remain undistorted, other system parameters such as the signal strengths or intensity ratios could become relevant for robust inference procedures, as well as auxiliary machine learning parameters. Two example spectra are shown in Figure 2b,c for the VIS spectrometer and NIR spectrometer respectively. The black vertical line shown in the NIR spectrum indicates the detection limit of that spectrometer.

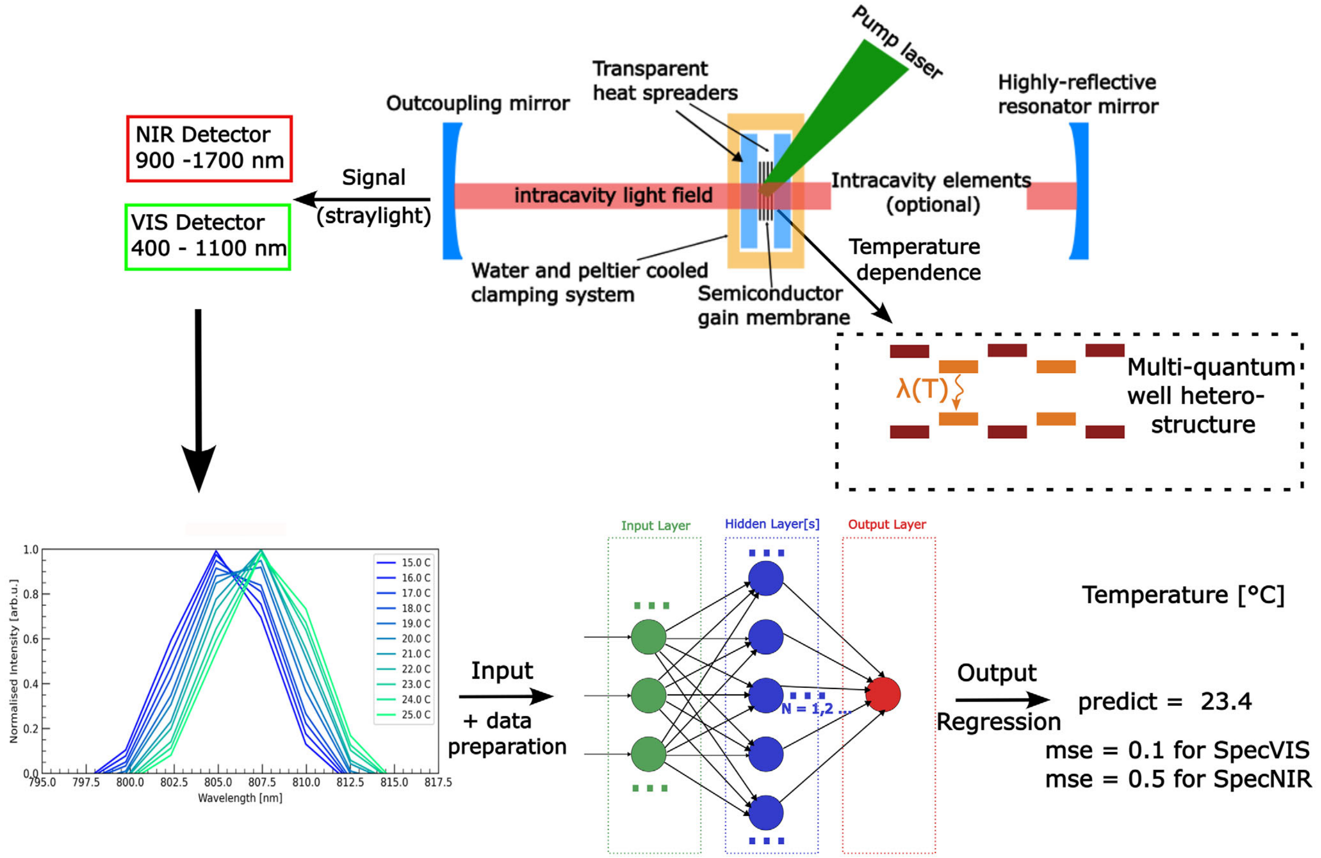

Figure 1. a) Sketch of the working principle. The laser signal from our employed semiconductor device is captured by spectrometers, two for the VIS and one for NIR spectral range. The captured spectra are prepared for insertion into the NN when matching the input layer structure. After training with labeled data, the few-layer NN model infers the temperature owing to a supervised learning technique. For a given input spectrum, a temperature value is deduced.

The laser system consisting of the MECSEL and the pump laser emits signals with different characteristics. While the MECSEL has a central wavelength of about 1075 – 1080 nm at considered operation temperatures with a full width half maximum (FWHM) of approximately 4.9 nm, the pump laser operates at a central emission wavelength of about 804 – 808 nm with a FWHM of 4.2 nm, according to our measurements with the VIS PEBBLEs. The FWHM is specified here at a temperature of 20 °C. The power curves of both lasers are depicted in the Appendix D. During the measurements of temperature dependent spectra the pump laser is operated at a output power of $P_{pump} \approx 9$ W, based on a fixed diode current. While the MECSEL can deliver output powers around 3 W at the 10 W pump level at room temperature when carefully readjusted, the here given power levels at 20 °C around 2.2 W (measured for the MECSEL at every spectrum acquisition process) could be maintained for a long working period without readjustment of the laser optics even after ramping the temperature between 15 and 25 °C multiple times. Note that the exact power measured may have varied slightly through different measurements the temperature changes, both in the chips and device environments, be it actively or passively induced through temperature controllers or environmental influences. According to the displayed representative power curves, the MECSEL system's electrical-input to optical-output efficiency is approximately 11 %.

The temperature of the pump laser is controlled by the water cooling/chiller system (model *MRC150/300, Laird Thermal Systems*[15]). The temperature of the MECSEL is controlled by the *thermo electric controller* (model *1091, Meerstetter engineering*[16]). Both temperatures can be set independently. For a given temperature range (here: 15 °C – 25 °C) the setup can automatically sweep through the temperatures in pre-defined steps and capture an arbitrary number of spectra for each temperature. Every spectrum recorded gets labelled with the corresponding temperature and the measured power of the laser. The laser power is measured with a power meter (model *PM100-A*, Thorlabs[17]) in the beam path behind the outcoupler mirror and behind a long-pass filter (edge around 850 nm).

For the training of the NN, spectra in the range from 15 °C to 25 °C in steps of 0.2 °C are recorded. In addition to the recorded data, auxiliary data are generated which incorporate shifted spectra (here shifted by ≈20 nm) to ensure that the absolute wavelength of the laser system does not matter during the testing and also for uncoupling the laser line's spectral position/signature from the detector pixel location. Note that the shift is applied to both laser lines accordingly. A corresponding noise part of the spectrum is copy-pasted to fill the side and complete the

ADVANCED SENSOR RESEARCH Open Access
www.advsensorres.com

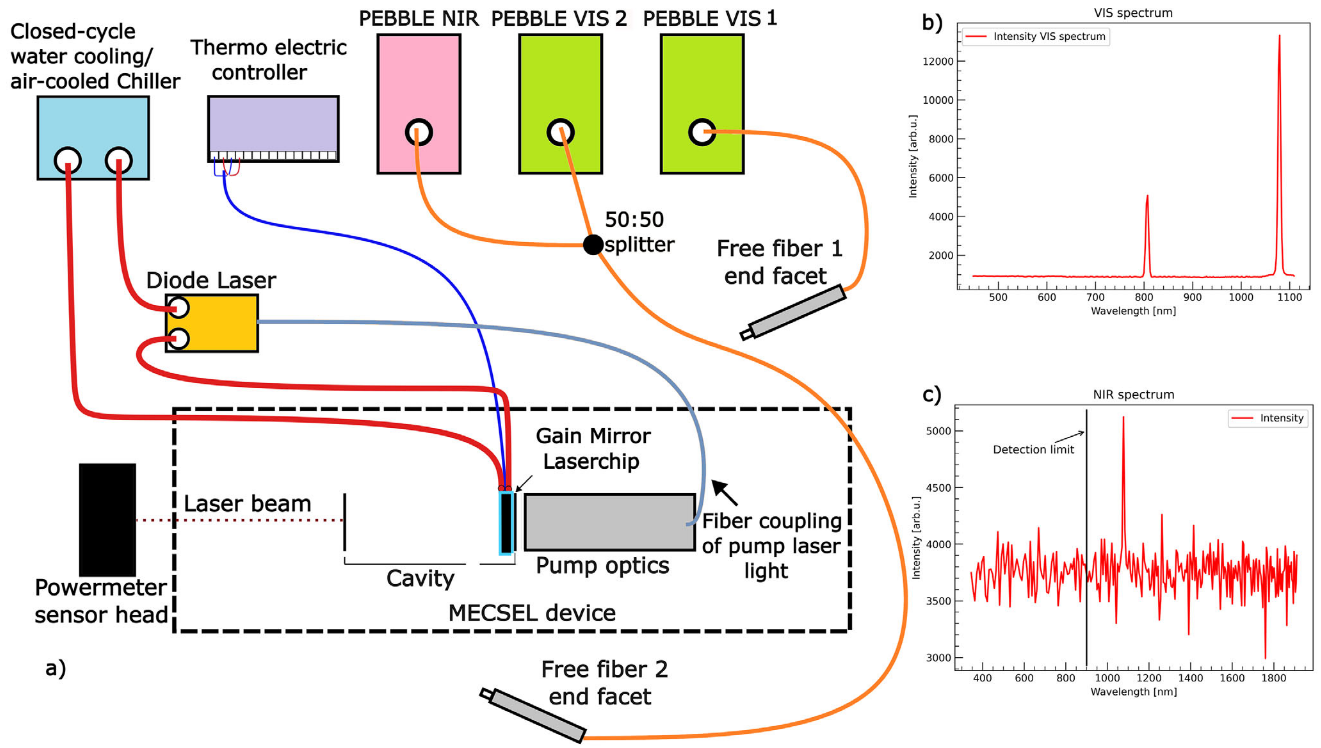

Figure 2. a) Sketch of the measurement arrangement for the acquisition of the laser system's spectral signature. Laser light is detected after back-scattering in free-space from an arbitrary screen (here power meter sensor head) by the fiber-coupled (orange lines) mini-spectrometers' detector for individual temperature settings. Here, the close-cycle water cooling (tubes drawn in red) and thermo-electric cooling device (wiring drawn in blue) act simultaneously for temperature control of the membrane gain chip, both adjusted and monitored software-wise. b) VIS raw spectra as recorded after the 50:50 (%) splitter on the respective fiber-coupled spectrometer (fiber 2). c) NIR raw spectra as recorded after the same beam splitter on the respective fiber-coupled spectrometer (NIR). The minimum detectable wavelength is indicated by a vertical black line at 900 nm.

spectral range of the captures to match that of original data. Real spectra and auxiliary data combined compose a set of approximately 268.000 spectra. However, only the 134.000 captured original spectra are used to train and test the model, whereas the shifted spectra are used to validate the model afterwards. The table in the results section with *mse* listings refers to the validation with these shifted spectra. For a better comparison, a reference table of the mse during the (self)-training is given in the Appendix in **Tables** A1 and A2, respectively.

To address the second crucial issue, that is, of preparing the data, **Figure** 3 indicates the preparation steps. In order to train the network efficiently, all spectra undergo the same preparation. Since a temperature change induces a shift in the emission signal spectrally, the absolute wavelength is not suitable for the inference of the temperature out of the given signal, as this can lead to the effect that in the sensor-deployment case an originally slightly de-tuned laser is interpreted as a shift of temperature, even though the change originates e.g from design, production or other technical differences for the same device category/chip type (thermal dependencies). To account for this, a reference spectrum at a chosen temperature, in this case 20 °C, is generated. The wavelength axis is then transformed to a relative spectrum using a central wavelength obtained from the reference spectrum. The reference value can for example be found by extracting the central emission wavelength with a Gaussian fit to the reference spectrum as depicted in Figure 3. The relative

Table A1. Results of the 5-layer deep network trained with the original recorded data prepared as explained in the main text. These *mse* were achieved by the model after the end of the learning process before the validation with the shifted data.

Learning Data	VIS				VIS + NIR			
Test Data	NIR	VIS	VIS 1	VIS 2	NIR	VIS	VIS 1	VIS 2
mse 0.2 °C steps	9.47	0.07	0.06	0.08	3.26	0.07	0.06	0.08
mse 0.5 °C steps	9.89	0.07	0.06	0.08	3.60	0.07	0.06	0.09
mse 1 °C steps	10.16	0.07	0.06	0.09	3.88	0.07	0.05	0.09

Table A2. Results 5-layer deep network trained with the data set containing only spectra without the pump laser. The data *mse* values were taken again from the last iteration of the learning process.

Learning Data	VIS				VIS + NIR			
Test Data	NIR	VIS	VIS 1	VIS 2	NIR	VIS	VIS 1	VIS 2
mse 0.2 °C steps	10.74	0.68	0.90	0.46	3.22	0.91	1.34	0.47
mse 0.5 °C steps	11.28	0.77	1.07	0.48	3.63	0.97	1.41	0.53
mse 1 °C steps	11.64	0.86	1.22	0.50	3.89	1.05	1.51	0.59

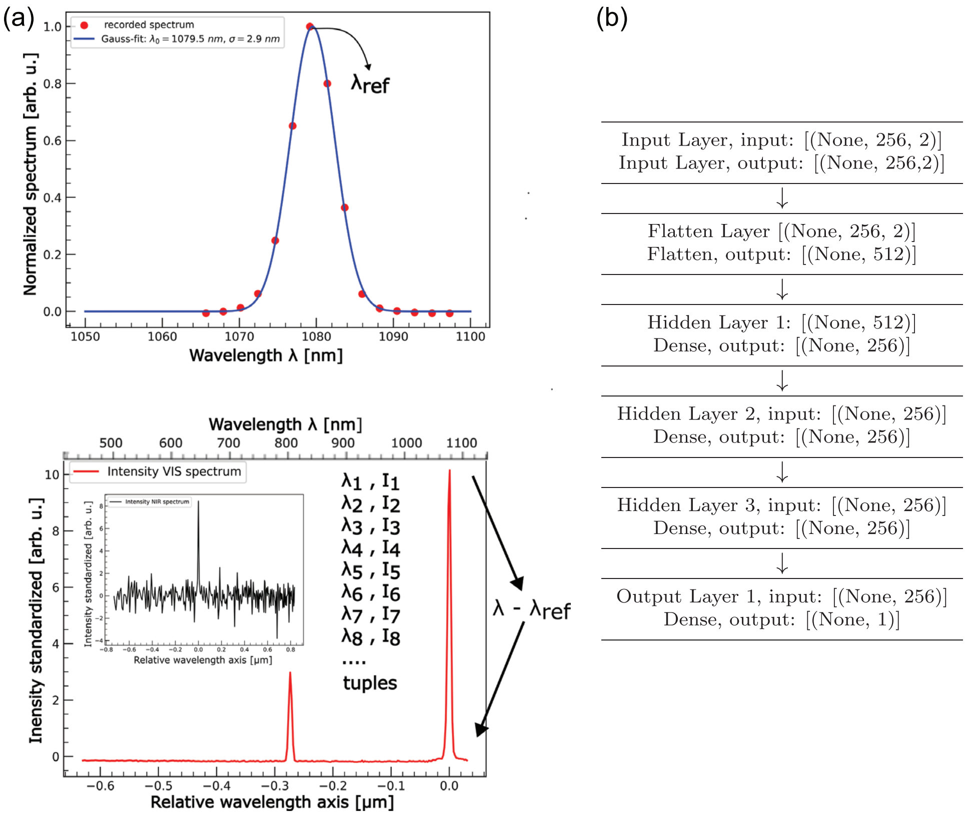

Figure 3. a) The reference wavelength is found by a Gaussian fit to the obtained spectra at the chosen reference temperature. Afterwards, the relative wavelength axis is generated. The obtained spectrum with the rescaled intensities exhibits the reference wavelength signal at 0. These data. i.e., the tuples of (relative) wavelength and intensity, become the input of the used ML model. b) Structure of the deployed 5-layer NN. The input layer is followed by a layer to flatten the 2 dimensional (D) input into a 1-D vector with alternating wavelength and intensity values (of type float numbers). The following three layers are fully-connected (dense) hidden layers with 256 units in each layer. The output layer consists of a single unit for the output of the temperature (float).

wavelength axis is then obtained according to the simple expression $\delta\lambda = \lambda - \lambda_{ref}$ where λ is the measured wavelength and λ_{ref} the reference value. The signal axis (i.e., the intensity counts) will then be rescaled such that its values have a mean of zero and a standard deviation of one. This ensures that all features have the same order of magnitude and, thus, the NN can fit the weights properly.[18] Afterwards, the counts and the corresponding wavelengths get combined so that one obtains 256 tuples (I_i/λ_i with counts and wavelength for each 256-entry long spectrum with i as pixel counter, i.e., array position). This 2D structure is the input to the NN. The first layer of the NN is a flatten layer to flatten the 2D structure of the input to a 1D vector with alternating wavelength and intensity entries.

3. Results and Discussion

For the training process a 5-layer deep NN with 3 hidden layers is used. The 5-layer NN was chosen through a *grid-search* from the python *scikit* module. Attention has been paid to both accuracy and computational resources, so that the 5-layer network appears more potent compared to shallower NNs of the same type but at the same time it is good enough that deeper architectures and complexity of the model appear unfavorable and not profitable, as the precision gain for more than 5 layer is low compared to the extra cost in computational effort. In addition, suitable hyperparameters are found with the same *grid-search*. In this work, the *sigmoid* activation function, 256 units in each hidden layer, 25 epochs (cycles of error minimization with Adam optimizer[19]) of learning and a batch size of 50 are used. Note that these parameters are only the best within the performed grid search and there might be even better combinations that were not checked here. For the training procedure, the originally recorded and input-prepared data set of 134.000 spectra is split into 70 % for training and 30 % for testing during the learning phase. The whole 20 nm shifted auxiliary data set of 134.000 spectra is used solely for (post-learning) performance testing, i.e., validation. The *mse* for different laser–spectrometer pairs in the validation process are summarized in **Table 1**. The left side of the table shows the *mse* when the model was trained with spectra from the VIS spectrometer only. On the right side, VIS and NIR spectra were used to train the model. The row "Test Data" shows which kind of spectra were used for testing or validation, e.g., from one or two different spectrometers ("NIR," "VIS1," "VIS2," or both VIS devices, short "VIS"). The three different step sizes (table rows) show the impact on the inference result when the temperature steps in sweeps are differently coarse for data used in the training and validation process. For comparison, the *mse* during the (self)-testing in the learning phase for the case "VIS + NIR" learning data and

Table 1. Performance test for the 5-layer deep network tested with a 20 nm shifted data set without retraining the network to the shifted spectra. The network is trained with the real recorded spectra only. For reference, the *rms*, that is the square root of the *mse*, is provided in the last row as well, since the *rms* is a typical measure for sensors. However, due to the Neural Net's inner handling of the value *mse* by its error function, the *mse* is referred to throughout the article. This allows directly comparing the error rate output from the training process with one's own performance tests with previously unseen spectra after training.

Learning Data	VIS				VIS + NIR			
Test Data	NIR	VIS	VIS 1	VIS 2	NIR	VIS	VIS 1	VIS 2
mse 0.2 °C steps	9.41	0.04	0.05	0.04	2.83	0.04	0.04	0.04
mse 0.5 °C steps	9.85	0.04	0.04	0.04	3.08	0.05	0.04	0.05
mse 1 °C steps	10.12	0.04	0.04	0.04	3.30	0.04	0.04	0.05
rms 1 °C steps	3.18	0.2	0.2	0.2	1.82	0.2	0.2	0.22

Table 2. Test for the 5-layer deep network trained with the same hyperparameters as above but this time the pump laser is artificially removed from the data. Afterwards, the relative shift was applied without retraining the network to the artificially altered spectra.

Learning Data	VIS				VIS + NIR			
Test Data	NIR	VIS	VIS 1	VIS 2	NIR	VIS	VIS 1	VIS 2
mse 0.2 °C steps	10.91	0.43	0.57	0.28	2.76	0.70	1.09	0.30
mse 0.5 °C steps	11.36	0.50	0.67	0.33	3.06	0.75	1.14	0.36
mse 1 °C steps	11.75	0.51	0.68	0.33	3.28	0.77	1.15	0.39

"VIS" testing data reached values as low as ≈0.06, which is similar to the *mse* obtained from the presented validation step. The validation solely relies on the auxiliary data with 20 nm shifted spectra after input preparation, without retraining the NN to the previously "unseen" shifted spectra. For comparison purposes, the *mse* obtained as a result of the learning procedure after the last training epoch is summarized in Table A1 (Appendix A).

When trained only with VIS spectra, the model has problems inferring from the NIR *PEBBLE* data, as expected. However, adding the NIR spectra to the training data improves the result significantly, when MECSEL data without pump line are part of the evaluation process. The VIS spectra reach an *mse* below 0.1 °C, while the NIR spectra remain in the range of ≈3 °C, in accordance to the influence of the spectrometers' resolving power, i.e., the capability of the used spectrometer to resolve the small shifts of the emission wavelength in the captured spectra. This indicates that a suitable spectrometer– laser pair should be used and that a calibration of the spectrometer–laser system might be helpful. In addition, the accuracy with the pump laser signal is higher compared to the MECSEL signal (linewidth diode pump laser ≈4.2 nm, linewidth MECSEL ≈4.9 nm, c.f. Appendix B). Accordingly, this results from the resolving power in combination with the linewidth of the laser lines. Because the linewidth of the pump laser is about 20 % narrower than the linewidth of the MECSEL, the trained NN can more accurately infer temperatures from the predominantly contributing pump laser signal; in simple words, the NN will likely focus on the line from which temperature-related behaviors are most obvious, the diode laser here. To test this hypothesis, a data set with artificially removed pump laser from the spectra is fed into the NN for the training, testing and validation of the network in the same way as before. The results of this check are given in **Table 2**. For a comparison to results directly obtained from the training procedure, a corresponding *mse* overview is given in Table A2.

Clearly, the *mse* become worse when excluding the pump laser line. This is understandable due to the fact that the pump laser line can be better resolved in the spectrometer, and thus, the shift can be detected more easily. Accordingly, temperature inference can become improved, or for broader lines worsened. As the validation data consists of shifted spectra, it is visible that the relative wavelength approach overcomes the bottleneck of the recorded "absolute" wavelength and ensures a temperature inference independent of the absolute wavelength. This enables a more versatile prediction of the temperature for a given spectrometer–laser pair configuration without transfer learning involved, e.g., accounting for production tolerances. Note that one can also train the network without the relative wavelength axis only with rescaled features. However, this limits the system to an absolute wavelength information. Nonetheless, when operating a stable laser system, where no major changes of the emission wavelengths (e.g., modejumps, production variations, power-induced shifts etc.) are expected, the inference of the temperature can be comparably precise as with the relative wavelength information. For a suitable laser– spectrometer pair with a reasonable resolving power of the laser emission line, in the case of involving the pump laser and absolute wavelength scale a *mse* of 0.13 °C is found. This is slightly worse than the primarily discussed approach, but still accurate enough for a range of possible use cases such as long time temperature monitoring where trends matter more than absolute temperatures. If the model is trained with heavier and more complex data sets featuring different laser signatures, e.g., with a removed pump laser or with data paying attention to power-dependent issues or other aspects of the signal properties, certain limitations could typically be overcome to some extent at the cost of computational load and data complexity. Correspondingly, in effect, we highlight here the advantage of a compact configuration and ressource effective approach. Moreover, smaller networks with less layers or less units can be used. However, this comes with the risk of reducing the precision a bit, or leading to a tendency of underfitting data, but it may well enable resource-saving in cases where this might be critical and accuracy is not the most important consideration. With a network consisting of 3 layers and 256 neurons in each layer a *mse* of ≈0.14 °C is found when trained with VIS + NIR data and tested with data from VIS PEBBLE 1, i.e., with data that contains both the MECSEL and pump laser line. Compared to the 5-layer network the accuracy dropped slightly but the model is still able to infer the temperature up to the first decimal point.

Instead of using a regressor network, one could also investigate the performance of a classifier network. In order to do so, one would need to group the temperatures into classes before training the network. This, however, has the limitation that the prediction (i.e., sensory) resolution is fixed as soon as the classes are fixed but enables to set the temperature resolution beforehand. Furthermore, long time laser signal observation could be utilized in future model developments to train such NNs to predict target property alterations, changes based on temperature changes and time-trace specialized network architectures could

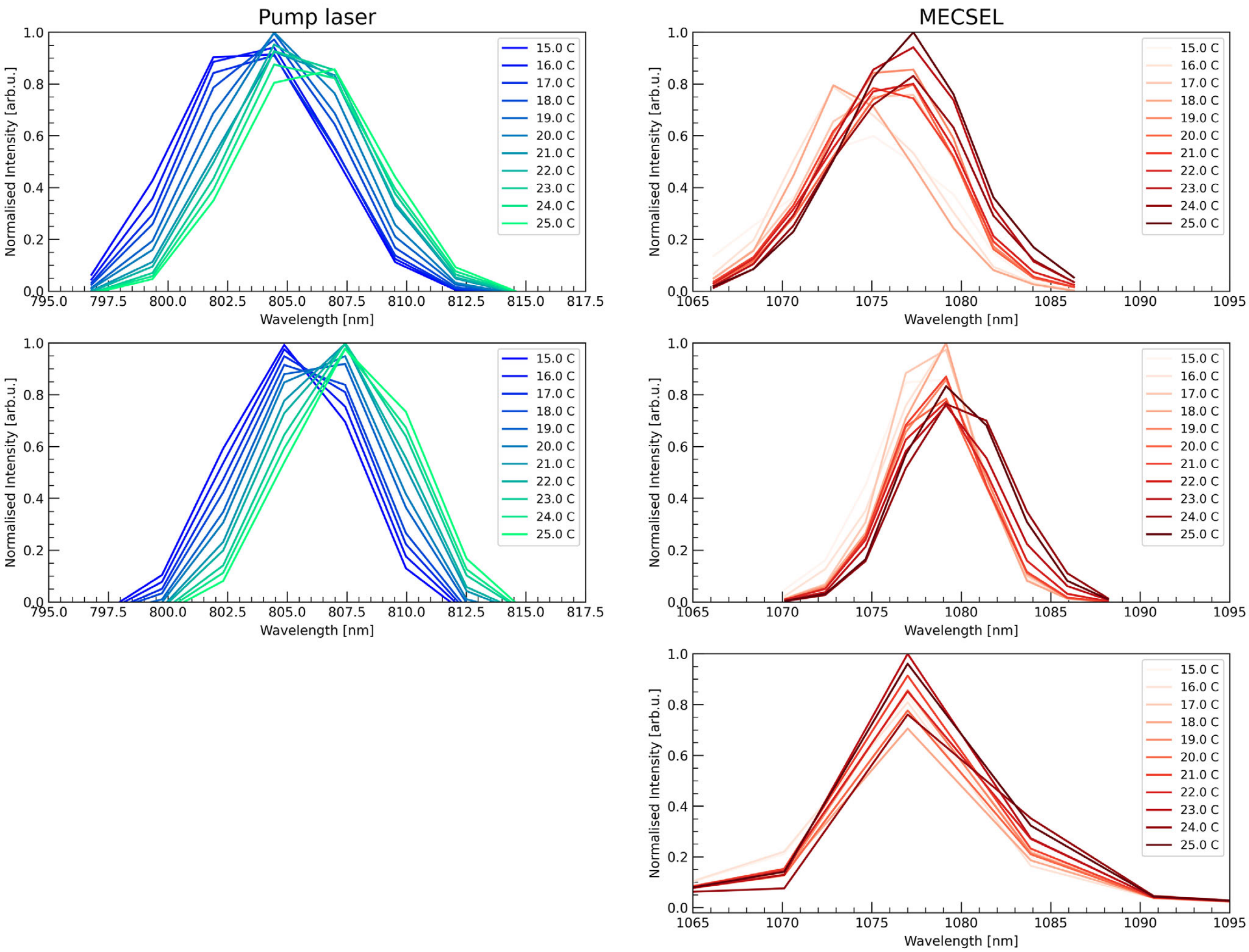

Figure B1. Averaged recorded intensity data shown in line spectra for temperatures between 15 °C and 25 °C. The sets of spectra are each normalized with respect to their highest occurring counts for the displayed temperature sweep. The individual color-code from dark to bright (blueish colors, pump laser, left column) and bright to dark (reddish colors, MECSEL, right column) indicates the change from a cold to a warm operation temperature. Each row corresponds to one of the spectrometers. The first row presents spectra captured by PEBBLE VIS 1, the second row those captured by PEBBLE VIS 2. The third row contains spectra recorded with the PEBBLE NIR. Because the NIR spectrometer cannot acquire the pump laser line, the last row only displays MECSEL signal.

lead to effective monitoring tools regarding external influences on selected emitter properties.

In addition to the here reported functionality, machine learning image-/video-analysis tools could be used to detect signal anomalies in time series. Through the flexibility of the ML models, they can be adjusted for the given device parameters, configurations and their applications, including in precision with respect to computational needs as well as application requirements.

If the application requires a broader temperature range than the here examined/presented, the range can be expanded by transfer learning of the existing NN, or by a new training of a machine-learning model with data sets covering wider temperate ranges. Furthermore, the use of a spectrometer with higher resolution with a capture of spectrally narrower emission would potentially improve the accuracy. Nonetheless, the method presented here aimed at enhancing the accuracy obtainable with cost-effective coarsely-resolving spectrometers due to the advantages of NNs, mainly pattern recognition abilities that enable reliable evaluation of noisy or sparse data (cf. Appendix C).

Besides applications in temperature sensing, such NN models can be used to investigate and infer other laser parameters (cf. recent examples in the field of laser examinations/ultrafast photonics by, e.g., D. Zibar et al.[20] and G. Genty et al.,[21] to name but a few), such as pulse duration or cavity parameters from spectral signatures of a laser system, benefiting from transfer learning capabilities for pre-trained models in combination with suitable and sufficiently large data sets.

4. Conclusion

We demonstrated a compact NN system with the capability to infer the temperature of two semiconductor lasers by a machine-learning method based on analysis of their recorded spectral signature. In combination with miniature spectrometers in the

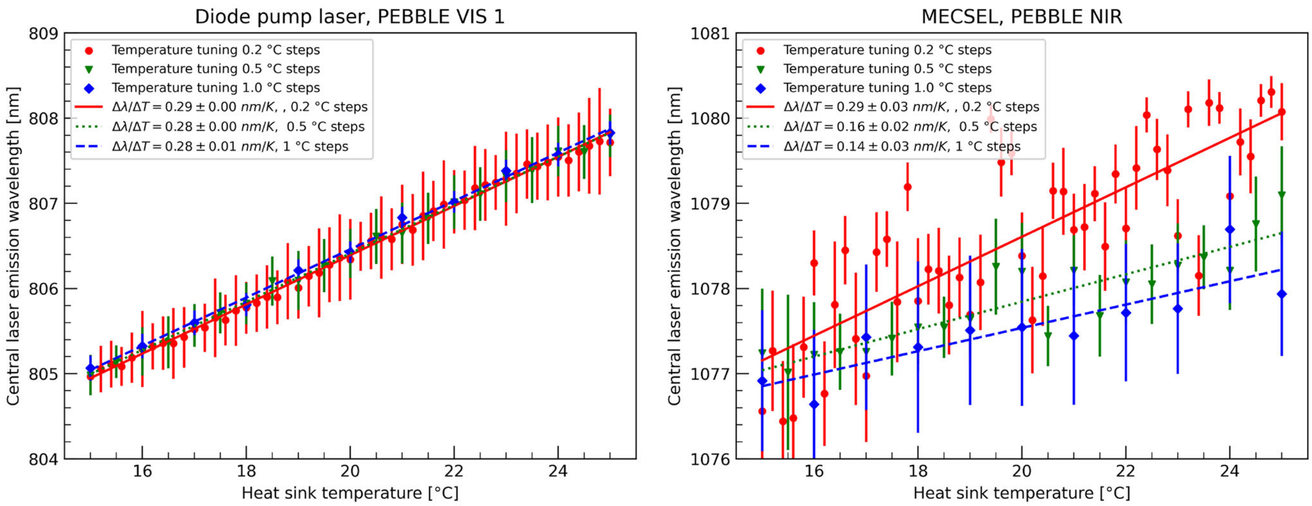

Figure C1. Example of a thermal shift coefficient determined for the diode pump laser and the MECSEL. The central wavelength was automatically extracted by a Gauss fit to averaged spectra from repeated recordings for each temperature setting. Error bars corresponding to the square root of the variance.

VIS and NIR spectral range with sufficiently high resolving power concerning the signal of interest, the accuracy reached as good as about 0.05 °C. This can be precise enough for possible remote/contactless sensing applications or for miniaturized emitter-based sensor elements with micro-spectrometers. This concept enables a non-contact and long-distance examination of a gain-medium temperature and therewith a pathway to semiconductor-technology based miniaturized sensor elements, which for instance can be remotely probed by merely a simple spectrometer coupled to a machine learning model.

Moreover, RecurrentNNs, RNNs, designed to remember sequences of inputs over longer periods can help to perform prediction tasks over longer periods, thereby enlarging the use cases of our study due to its ability to recognize temporal evolution. By capturing temperature temporal dependencies, real-time application of the machine learning model with signals/systems varying dynamically over time could be addressed effectively. Combined with the ability of ConvolutionalNNs, CNNs, to extract spatial features, spectral monitoring could be done with known correlations between sensor signals and different environmental impacts, improving the ability to differentiate between multiple wavelength shift causes sufficiently for a given application scenario.

Appendix A: Comparison Tables for the Mean-Squared-Error Values

For comparison to the validation Tables 1 and 2 given in the results section, here the *mse* during the self testing at the end of the learning process is provided. The hyperparameters (epochs, optimizer, batch size etc.) of the model as well as the data input preparation (rescalings) are the same.

When comparing these values with the validation values, it can be seen that the validation *mse* is even below the one for the in-training testing. This most likely originates from the fact that the validation data set with 134.000 auxiliary spectra contains significantly more data points than the in-training test set, which is made up of only 30 % of the 134.000 (original) spectra. Thus, the spread reduces and high *mse* values tend to lose their impact resulting in a lower *mse*.

Appendix B: Representative Temperature-Tuned Spectra

Here, spectra indicating the spectral shift from bright to dark colors, between 15 and 25 °C, for the diode laser (left) and for the MECSEL (right) are shown in **Figure B1**. The first row is captured by the VIS spectrometer 1, the second by VIS spectrometer 2 and the last by the NIR spectrometer. The linewidth is obtained through averaging all recorded spectra for the same temperature setting and applying a Gauss fit to it, from which the FWHM value is extracted as the linewidth. For the here used laser systems, the linewidth is ≈4.2 nm and ≈4.9 nm for the diode laser and the MECSEL, respectively.

Appendix C: Thermal Shift Coefficient

In order to display the benefits of the NN approach compared to the well known technique of fitting the emission peak by, e.g., a Gauss fit to get extracted central emission wavelengths of the laser plotted against the temperature for the consecutive determination of a laser's thermal shift coefficient, two examples for our spectrometers are given in **Figure C1**. It can be seen that with our devices (spectral resolution around 8 nm and 12 nm for these VIS and NIR spectrometers according to their product specifications, respectively) the coefficient extraction can be ambiguous, as the error bars obtained as the square root of the variance of each data point (averaged spectra) are relatively large for both lasers.

To obtain an average thermal shift coefficient for each laser, all spectrometers were used to obtain the respective coefficient as averaged over all spectrometers to become 0.25 ± 0.08 nm/K for the MECSEL, and 0.27 ± 0.02 nm/$K$for the diode laser, where the errors represent the standard deviation from the average. This on the one hand indicates that the extracted thermal shift coefficient can deviate within different series recorded at different temperature increment rates, as shown in in the Figure C1. On the other hand, there are also minor deviations among recorded coefficients when evaluating spectra of the individual spectrometers employed, concerning the standard deviations spanning about 10–30% of the mean value. Accordingly, extracting meaningfully precise thermal shift coefficients for later reference use can be a challenge. To achieve such properly,

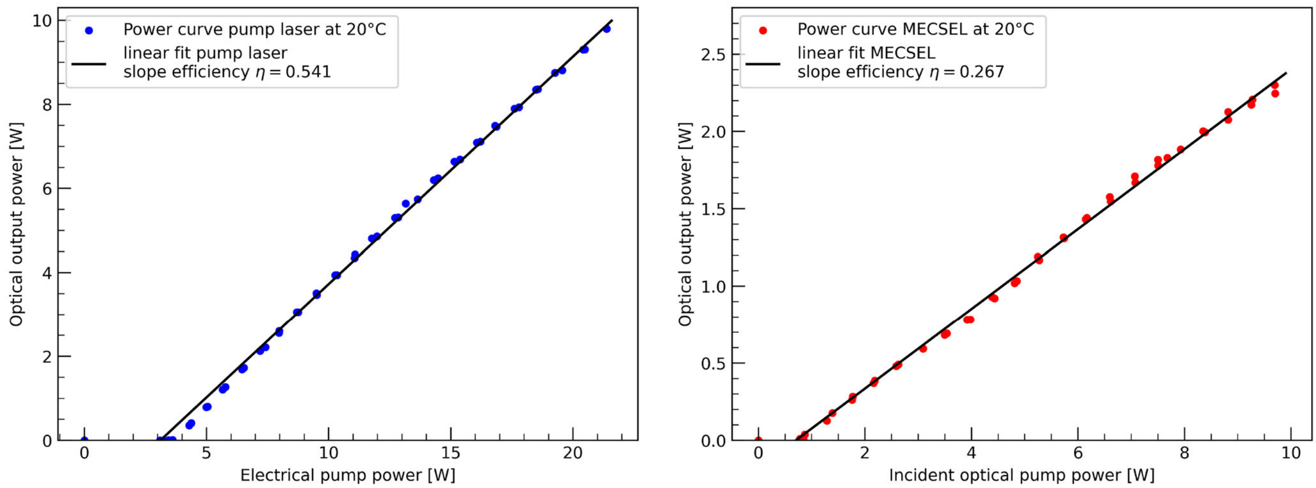

Figure D1. Representative input–output power curves of the pump laser (left) and the MECSEL (right) obtained at a time before conducting the experiment. The slope efficiency of the diode laser is approximately 54.1 %, while the slope efficiency of the MECSEL is approximately 26.7 %. The lasing thresholds for the pump laser and the MECSEL are approximately 3.1 W and 0.9 W, respectively. The input power to the MECSEL corresponds to the output power of the pump laser.

a spectrometer with sufficiently high resolution and a stable laser with well defined temperature behavior is needed. In contrast, the machine-learning based input–output mapping method with NNs presented here, however, allows non-contact remote sensing even with the compact, robust, mobile and cost-effective devices, additionally not restricting the user to strictly linear temperature responses – neither over smaller nor larger examination ranges.

Appendix D: Power Curves of the MECSEL and the Pump Laser

Representative power curves (P_{in} vs. P_{out}) of the MECSEL laser and the pump laser are provided here, additionally. This gives an overview of the input–output characteristics. Both power curves were measured at a temperature of 20 °C and the input power is first ramped up form 0 to 10 W and then ramped down again. The electrical power input to the pump laser is provided by a DC power supply. The lasing output from this diode laser (detected after the pump optics by a thermal power-meter sensor head) becomes the incident optical pump power of the MECSEL. The lasing thresholds for the pump laser and the MECSEL are approximately 3.1 W and 0.9 W, respectively **Figure D1**.

Acknowledgements

Financial support by the Deutsche Forschungsgemeinschaft (German Research Foundation, DFG: RA2841/12-1)—Projektnummer 456700276—is acknowledged.

Conflict of Interest

The authors declare no conflict of interest.

Author Contributions

A.R.-I. conceived the experiment and guided J.M. on the machine learning project. Data acquisition and preparation was conducted by J.M. The multilayer-neural-network model for the sensing application was jointly realized by J.M. and A.R.-I. The supervised-learning model configurations and their performance were examined by J.M. The results were discussed and summarized in a manuscript by both authors.

Data Availability Statement

The data that support the findings of this study are available from the corresponding author upon reasonable request. Also, see dataset publication by J. Mannstadt and A. Rahimi-Iman, "Dataset'Towards Neural-Network-based Optical Temperature Sensing of Semiconductor Membrane External Cavity Laser'". *Zenodo*, **2025**, Apr. 22, 15262006, https://doi.org/10.5281/zenodo.15262006.

Keywords

artificial neural network, machine learning, semiconductor laser, supervised learning, temperature sensor

Received: November 22, 2024
Revised: April 22, 2025
Published online: June 9, 2025

[1] O. S. Wolfbeis, *Anal. Chem.* **2006**, *78*, 3859.
[2] E. Vavrinsky, N. E. Esfahani, M. Hausner, A. Kuzma, V. Rezo, M. Donoval, H. Kosnacova, *Biosensors* **2022**, *12*, 217.
[3] I. Ashry, Y. Mao, B. Wang, F. Hveding, A. Bukhamsin, T. K. Ng, B. S. Ooi, *J. Lightwave Technol.* **2022**, *40*, 1407.
[4] F. Khan, Z. Xu, J. Sun, F. M. Khan, A. Ahmed, Y. Zhao, *Sensors* **2022**, *22*, 3310.
[5] B. Lee, *Opt. Fiber Technol.* **2003**, *9*, 57.
[6] V. K. Rai, *Appl. Phys. B* **2007**, *88*, 297.
[7] B. Heinen, F. Zhang, M. Sparenberg, B. Kunert, M. Koch, W. Stolz, *IEEE J. Quantum Electron.* **2012**, *48*, 934.
[8] R. G. Bedford, M. Kolesik, J. L. A. Chilla, M. K. Reed, T. R. Nelson, J. V. Moloney, *Proc. of SPIE*, Orlando, Florida, USA **2005**, 199, http://proceedings.spiedigitallibrary.org/proceeding.aspx?doi=10.1117/12.607428.
[9] Y. Xiao, X. Zhang, J. Li, Laser Crystal Temperature Measurement Method and Devic, Electronic Equipment and Storage Medium, China CN116608970A, **2023**.
[10] A. Rahimi-Iman, J. Mannstadt, Verfahren zur Temperaturbestimmung eines Lasermediums, Germany EP23215184.5, **2023**.

[11] IBSEN Photonics, spectrometer manufacturer, **2023**, https://ibsen.com/products/oem-spectrometers/pebble/.
[12] IBSEN Photonics, PEBBLE VIS-NIR, **2023**, https://ibsen.com/productinfo/pebble-vis-nir/#_info.
[13] IBSEN Photonics, PEBBLE NIR, **2023**, https://ibsen.com/productinfo/pebble-nir/?portfolioCats=4666%2C4664%2C4665.
[14] Twenty-one Semiconductors GmbH Membrane External Cavity Laser system MEXL, **2024**, https://www.21semiconductors.com/.
[15] Laid thermal system thermosystem MRC 150/300 benchtop recirculating chiller, **2023**, https://lairdthermal.com/sites/default/files/ckfinder/files/resources/Manuals/MRC-Chillers/MRC-150-300/MRC150-300-User-Manual-rev12.pdf.
[16] Meerstetter engineering, thermo-electric controller TEC-1091, **2023**, https://www.meerstetter.ch/products/tec-controllers/tec-1091.
[17] Thorlabs, sensorhead powermeter PM 100-A, **2023**, https://www.thorlabs.com/thorproduct.cfm?partnumber=PM100A.
[18] C. M. Bishop, *Review of Scientific Instruments* **1994**, *65*, 1803.
[19] D. P. Kingma, J. Ba, Adam: A Method for Stochastic Optimization, **2014**, https://arxiv.org/abs/1412.6980, Version Number: 9.
[20] D. Zibar, J. Thrane, J. Wass, R. Jones, M. Piels, C. Schaeffer, in *Optical Fiber Communication Conference*. OSA, Anaheim, California, ISBN 978-1-943580-07-1, **2016** Tu3K.1, https://opg.optica.org/abstract.cfm?URI=OFC-2016-Tu3K.1.
[21] G. Genty, L. Salmela, J. M. Dudley, D. Brunner, A. Kokhanovskiy, S. Kobtsev, S. K. Turitsyn, *Nat. Photonics* **2021**, *15*, 91.